Protein Conformation and Dynamics. Effects of Crankshaft Motions on ^{1}H NMR Cross-Relaxation Effects

Hélène Déméné*,[†] and Istvan P. Sugàr[‡]

Departments of Biomathematical Sciences and Physiology & Biophysics, The Mount Sinai School of Medicine, New York, New York 10128, and Centre de Biochimie Structurale, 15 avenue Charles Flahault, 34060 Montpellier Cedex 2, France

Received: March 5, 1999

In this paper, the slow backbone motions for segments of interleukin 1β and calbindin D_{9k} are characterized and the effects of these motions on the interproton cross-relaxation effects are investigated. We assume that the flexible loop segments are involved in three motions: fast librational vibrations, slow crankshaft motions, and the overall tumbling motion of the protein. The parameters characterizing the conformers and dynamics (amplitude and time scale) of the flexible segments are estimated by fitting the calculated data to the experimental heteronuclear ^{15}N relaxation data. NOESY spectra simulated by using the flexible model are in better agreement with the experimental data than those simulated by using the rigid model. Neglecting flexibility may cause biases in the estimated interproton distances derived from cross-relaxation peaks by up to 1 Å.

1. Introduction

The recognition of the "induced fit mechanism" of enzyme−substrate interaction made it obvious that conformational flexibility of biomolecules is crucially important to their function. Thus determination of the conformation and dynamics of the flexible parts of a biomolecule is an important step toward a better understanding of its activity.[1]

Currently, NMR spectroscopy is one of the most powerful techniques for the investigation of both the conformation and dynamics of proteins at an atomic level. However, NMR dynamical and structural studies remain rather separated. Usually, the conformation of a protein is determined from the homonuclear dipolar relaxation rates present on NOESY-type spectra, while the dynamics of the flexible regions are inferred from measurements of heteronuclear relaxation rates of backbone atoms (^{15}N or [13]Cα). As a result, conformational flexibility identified from heteronuclear NMR relaxation data is ignored during the structure calculation process from NMR homonuclear proton relaxation rates. Taking into account both types of information (homo- and heteronuclear rates) in an energetic cost $\Sigma(P_{calc} - P_{exp})^2$ supposes the ability to simultaneously (back-)calculate them and represents undoubtely the major difficulty. Up to now, the back-calculation methods of heteronuclear and dipolar proton−proton rates in the case of internal motions are inadequate for this purpose from our point of view. We will first briefly review them and discuss their inconveniences before presenting our strategy.

Available Methods for Back-Calculation of Homonuclear Proton Relaxation Rates. One method assumes "slow exchange" (as compared to the overall correlation time of the molecule) between conformations. Depending on the ratio between the longitudinal relaxation time and the interconversion rate,[2] the back-calculated NOE's are derived from a treatment

of the relaxation matrix similar to that of chemical exchange[2,3] or are taken to be proportional to $\sum_i \alpha_i/r_i^6$ where r_i is the interproton distance in the *i*th conformer and α_i its proportion.[4] In this method a set of conformers is generated whose calculated averaged proton nuclear Overhauser effects match the experimental ones. The validation of these conformers is then problematic, since a sufficiently large number of conformers may satisfy all the experimental data without being relevant. Furthermore, the time scale of the interconversion of conformers covers only a limited region of the lower time scale of motions investigated by NMR heteronuclear relaxation (exchange contribution to the transversal relaxation rate R_2).

Lipari and Szabo[5] introduced parameters of the *model-free approach* that characterize the dynamics of each interatom vector. The limitation of the method is that, in the case of interproton vectors, these parameters can be obtained only from long molecular dynamics (MD) simulations.[6] The capacity of the currently available supercomputers sets the upper limit of length of MD to the nanosecond range for middle-sized proteins, which restricts the time scale of the investigated internal correlation time for interproton vectors to the tenth, i.e., "fast motion" in terms of heteronuclear relaxation data (picosecond). In addition, this method generally overestimates the flexibility of mobile and solvent-exposed segments of proteins.

The final method introduced time-averaged restraints.[7] The disadvantage of this approach is again the limited computational power, and thus the conformational transitions can be investigated only in the fast motion limit.

Available Methods for Back-Calculation of Heteronuclear Relaxation Rates. The first back-calculation method computes the heteronuclear relaxation rates from the time course of a MD simulation, encountering the problem of computer capacity mentioned above.[8,9]

The second method calculates the NMR heteronuclear relaxation data from a physically relevant model of motion. Analytic forms of relaxation rates have been derived for a large number of physical models since the early times of relaxation studies.[10] However, since the number of unknown parameters

---

* Corresponding author. Fax: (33) 4 67 52 96 23. E-mail: helene.demene@cbs.univ-montp1.fr.
[†] Centre de Biochimie Structurale.
[‡] Mount Sinai School of Medecine.

Protein Conformation and Dynamics

J. Phys. Chem. A, Vol. 103, No. 24, 1999 **4665**

describing these models may be very large, and the amount of experimental relaxation data is very limited, the discrimination of physical models based only on experimental data is a largely underdetermined problem.

The model-free approach[5] is an alternative, convenient method to interpret the experimental heteronuclear relaxation data of backbone atoms (^{15}N and ^{13}Cα), without using a specific model of motion. This approach describes internal dynamics with generalized order parameters and correlation times of the N−H or Cα−H spin pairs. In addition to the overall correlation time of the protein, most relaxation parameters of residues located in the rigid parts of proteins can be described by two parameters of librational motions, τ_{fast} (ps), which represents an internal correlation time, and S_{fast}^2, which characterizes the spatial restriction of the vector's motion. Extension of the dynamical information obtained from heteronuclear relaxation data about an H−X bond using such an approach to the dynamics of ^{1}H−^{1}H vectors is not straightforward. Recently, LeMaster[11] pointed out that these small amplitude, fast motions do not significantly distort the interatomic distance determination. However, to characterize the relaxation of backbone atoms located in flexible loops, one may have to include two additional parameters, τ_{slow} (100 ps to nanoseconds) and S_{slow}^2 characterizing a much slower motion with a larger amplitude ($S_{slow}^2 < S_{fast}^2$),[12] whose effects are yet to be characterized.

Strategy for Simultaneously Calculating Heteronuclear and Proton Homonuclear Relaxation Rates in the Nanosecond−Picosecond Range. MD simulations were able to provide qualitative if not totally satisfactory quantitative information about the types of intramolecular motions. For protein backbone atoms, such as the N and Cα atoms, MD simulations have discriminated between two kinds of relaxation-active processes: well-characterized fast motions in the subpicosecond and picosecond time scale, which are referred to as "librational vibrations", and slower motions on a much larger time scale from tens of picoseconds to 100 ps and more. These slower motions are usually too slow to be quantitatively characterized by MD simulations. However, a considerable number of reported MD simulations seem to indicate that most of the time, the slower motions are crankshaft-type flips, i.e., anticorrelated variations of neighbor backbone dihedral angles ψ_{i-1} and ϕ_i of the ith residue, so that the quantity $\psi_{i-1}(t) + \phi_i(t)$ remains constant.[8,13] Fushmann et al.[8c] have shown that when these flips are present, they contribute to 70−80% of the relaxation of the respective ^{15}N−^{1}H vectors. These crankshaft flips appear to occur in flexible loops connecting the more rigid subunits of the protein. Residues located within the most rigid parts of the protein such as helices and β sheets experience only the spatially restricted fast librational motion and the slow overall tumbling motion of the protein.

In this paper a quantitative characterization of the slow, backbone crankshaft motions is presented and their effects on proton−proton cross-relaxation are investigated. Section 2 presents the theoretical basis for calculating heteronuclear and proton−proton relaxation rates. The spectral density of the interproton vectors is calculated by assuming anticorrelated jumps (crankshaft motions) between conformations. The parameters of these jumps (amplitude and frequency) are derived from the heteronuclear experimental relaxation parameters ^{15}N R_1 and ^{15}N R_2 and steady-state NOE, {^{1}H}−^{15}N NOE.

In section 3, the conformation and dynamics of a flexible segment of interleukin 1β and calcium-loaded calbindin are determined. Interleukin 1β and calbindin D$_{9k}$ are 151 and 75 amino acid long proteins, essentially composed of β sheets and

helices, respectively. The results show that (i) backbone flexibility significantly affects only the weakest NOEs and (ii) simulated NOESY spectra are in better agreement with the experimental spectra when our model of flexible backbone segments is used than when the rigid model is used. For both proteins, distance determination is found to be significantly biased for the weakest NOEs, whereas the effects of backbone flexibility on the strong NOEs can be neglected.

2. Back-Calculation of NOESY Spectra of Flexible Proteins by Using ^{15}N NMR Relaxation Parameters

For the sake of simplicity we confine ourselves to the treatment of the relaxation of ^{15}N backbone atoms, but our observations and protocol are valid for Cα atoms as well.

2.1. General Expressions for NMR Heteronuclear and Homonuclear Relaxation Rates. At high field, the relaxation of the ^{15}N backbone atom is governed by the dipolar interaction with its bound ^{1}H atom and by its chemical shift anisotropy $\Delta\sigma_{||}$.[14] The relaxation rate constants, R_1 (spin−lattice or longitudinal relaxation) and R_2 (spin−spin or transverse relaxation), and the steady-state NOE, {^{1}H}−^{15}N NOE, are given by

$$R_1 = \{d^2/10[J(\omega_H - \omega_N) + 3J(\omega_N) + 6J(\omega_H + \omega_N)] + {}^2/_{15}c^2 J^{red}(\omega_N)$$

$$R_2 = \{d^2/20[4J(0) + J(\omega_H - \omega_N) + 3J(\omega_N) + 6J(\omega_H) + 6J(\omega_H + \omega_N)] + {}^2/_{15}c^2({}^2/_3 J^{red}(0) + {}^1/_2 J^{red}(\omega_N)) \quad (1)$$

$$NOE = 1 + \{d^2\gamma_H/(R_1\gamma_N)\}[6J(\omega_H + \omega_N) - J(\omega_H - \omega_N)]$$

where

$$d = [\mu_0/(4\pi)]\gamma_H\gamma_N\hbar$$

$$c = \gamma B_0 \Delta\sigma_{||}$$

The ^{15}N chemical shift tensor is assumed to be symmetric with $\Delta\sigma_{||} = -160$ ppm.[15] In eqs 1, $J(\omega)$ is distance dependent, whereas $J^{red}(\omega)$ is not (see eq 3).

The chemical shift anisotropy of the proton is small enough to be safely neglected. As a consequence, the relaxation processes of protons are dipolar in nature and result in the following measurable relaxation parameters for a given proton H, where the summation is taken over all other protons H′:

$$R_{1H} = ([\mu_0/(4\pi)]\gamma_H^2\hbar)^2/10\sum_{H'} [J(\omega_{H'} - \omega_H) + 3J(\omega_H) + 6J(\omega_H + \omega_{H'})]$$

$$R_{2H} = ([\mu_0/(4\pi)]\gamma_H^2\hbar)^2/20\sum_{H'} [4J(0) + J(\omega_H - \omega_{H'}) + 3J(\omega_H) + 6J(\omega_{H'}) + 6J(\omega_H + \omega_{H'})] \quad (2)$$

$$\sigma_{HH} = ([\mu_0/(4\pi)]\gamma_H^2\hbar)^2/10[6J(\omega_H + \omega_{H'}) - J(\omega_{H'} - \omega_H)]$$

Equations 2 are strictly valid for nonlike spins, which is true for the class of protons investigated here. In eqs 1 and 2, the spectral density functions, $J(\omega)$ and $J^{red}(\omega)$, are given by the cosine Fourier transform of the orientational correlation function for a vector joining the two relevant atoms involved in the dipolar interaction and for a unit vector along the principal axis of the symmetrical chemical shift tensor, respectively. In the case of amide ^{15}N−^{1}H atoms, the direction of these two vectors

is identical. As a result, the spectral densities in eqs 1 can be calculated with

$$J^{\text{red}}(\omega) = r_{\text{HN}}{}^{6}J(\omega) \qquad (3)$$

Let us consider an isotropic protein molecule. We assume that the correlation function of an internuclear vector ([1]H−[15]N or [1]H−[1]H) can be factored as follows:

$$C(t) = \exp(-t/\tau_{\text{c}})C_{\text{jump}}(t)\,C_{\text{librational}}(t)$$

where the first factor describes the overall tumbling motion of the protein with a correlation time τ_{c} and the second factor describes jump dynamics between discrete conformers of the protein. The third factor refers to the fast, small amplitude librational motions and can be modeled according to Lipari and Szabo[5] with a generalized order parameter and an internal correlation time $S_{\text{fast}}{}^2$ and $\tau_{\text{fast}}{}^2$, respectively. The Fourier cosine transform of the correlation function, $C(t)$, results in the spectral density function, $J(\omega)$:

$$J(\omega) = S_{\text{fast}}{}^2 J_{\text{jump}}(\omega, \tau_{\text{c}}) + (1 - S_{\text{fast}}{}^2)J_{\text{jump}}(\omega,\tau) \qquad (4)$$

where $\tau = \tau_{\text{fast}}\tau_{\text{c}}/(\tau_{\text{fast}} + \tau_{\text{c}})$ and from ref 16 eq 14.1:

$$J_{\text{jump}}(\omega, \tau_{\text{c}}) =$$

$$(4\pi/5)\tau_{\text{c}}/(1 + \omega^2\tau_{\text{c}}{}^2) \sum_{n=-2}^{2} \left| \sum_{i=1}^{N} \langle P_i \rangle Y_{2n}(\Phi_i^{\text{mol}})/r_i^3 \right|^2 +$$

$$\sum_{i,j=1}^{N} \sum_{k=1}^{N-1} (4\pi/5)\tau_k/(1 + \omega^2\tau_k{}^2)\langle P_i \rangle \sum_{n=-2}^{2} c_{ij}^{(k)} Y_{2n}(\Phi_i^{\text{mol}})Y_{2n}^{*}(\Phi_j^{\text{mol}})/$$

$$(r_i^3 r_j^3) \quad (5)$$

where N is the number of conformations, r_i is the internuclear distance in the ith conformation, $\langle P_i \rangle$ is the probability of finding the molecule in the ith conformation at equilibrium, $Y_{2n}(\Phi_i^{\text{mol}})$ are the second rank spherical harmonics normalized according to Rose,[17] Φ_i^{mol} specifies the polar angles of the internuclear vector in the ith conformation in a frame attached to the molecule, λ_k and c_{ij}^k are related to the eigenvalues and eigenvectors of the rate constant matrix, **T**, and $\tau_k^{-1} = \tau_{\text{c}}^{-1} + \lambda_k$.

The IJth off-diagonal element of this matrix is $T_{IJ} = \nu_{IJ}e^{(E_J - E_I)/2kT}$, where ν_{IJ} is the number of trials for jump from the Jth to the Ith conformation per unit time, while E_I is the energy of the molecule in the Ith conformation. The diagonal element is calculated from the off-diagonal elements with $T_{II} = -\sum_{J \neq I}T_{JI}$.

If the librational vibrations are much faster than the tumbling motion and each of the jumps (i.e., $\tau_{\text{fast}} \ll \lambda_i^{-1}$ for every i and $\tau_{\text{fast}} \ll \tau_{\text{c}}$), then $J_{\text{jump}}(\omega, \tau_{\text{c}}) \gg J_{\text{jump}}(\omega, \tau_{\text{fast}})$. By means of this approximation, the spectral density and the relaxation parameters are

$$J \approx S_{\text{fast}}{}^2 J_{\text{jump}}(\omega;\tau_{\text{c}})$$

$$R_{i,\text{exp}} \approx S_{\text{fast}}{}^2 R_{i,\text{jump}} \qquad (6)$$

$$\text{NOE}_{\text{exp}} \approx \text{NOE}_{\text{jump}}$$

where $R_{1,\text{jump}}$, $R_{2,\text{jump}}$, and NOE_{jump} are calculated by using eqs 1 and the spectral densities J, by using eqs 5.

2.2. Back-Calculation of the Heteronuclear Relaxation Rates Using the Jump Formalism. Flexible segments can be identified by interpreting the ^{15}N NMR relaxation data by using

the model-free approach. Relaxation rates of the backbone amide groups in the flexible segments, such as residues Gln32-Gly33-Glu34-Asp35-Met36 for protein interleukin 1β and Lys41-Gly42-Gly43-Ser44 for protein calbindin D$_{9k}$, cannot be described by means of the original model-free approach; however, an extended version of the model-free approach can be used, which interprets the relaxation data in terms of τ_{c}, τ_{slow}, $S_{\text{slow}}{}^2$, and $S_{\text{fast}}{}^2$.[18,19] In the case of these two flexible segments, MD simulations strongly suggest that the slow motion processes are crankshaft type motions,[8,9] confirming the initial interpretation of the relaxation data for these residues in terms of a two-state jump model by Clore et al. Clore et al. also calculated the corresponding angle of jump, φ, for the HN vector. However, this calculated φ angle is the relaxation active angle of the HN vector, which is different from the angle of jump, θ, of the backbone torsion angles. To obtain the θ angle, for each residue i two conformations are generated from the average minimized NMR structure[20] by introducing a distortion of jump amplitude θ_i to the backbone dihedral angles ϕ and ψ:

$$\psi_{i-1}^{\text{l}} = \psi_{i-1}^{\text{ave}}, \qquad \phi_i^{\text{l}} = \phi_i^{\text{ave}}$$
$$\psi_{i-1}^{2} = \psi_{i-1}^{\text{ave}} - \theta_i; \quad \phi_i^{2} = \phi_i^{\text{ave}} + \theta_i \qquad (7)$$

where superscript "ave" refers to the average minimized structure of the flexible segment and superscripts 1 and 2 to the conformers of each residue within the flexible segment. Interconversion between conformers 1 and 2 is then a crankshaft type motion. Both conformers were superimposed on the original average conformation, here conformer 1. The amplitude θ_i and frequency ν_i of the jump between conformers 1 and 2 were obtained by fitting the calculated data $R_{1,\text{jump}}^i$, $R_{2,\text{jump}}^i$, $\text{NOE}_{\text{jump}}^i$ to the experiment-derived data ($R_1^i/S_{\text{fast}}^i{}^2$, $R_2^i/S_{\text{fast}}^i{}^2$, NOE^i). The parameters τ_{c} and $(S_{\text{fast}}^i)^2$ are known from refs 18 and 19. In our calculations we assumed similar conformer energies. The fitting was individually performed for the residues 41, 42, 43, and 44 of calbindin and for the residues 32, 33, 34, 35, and 36 of interleukin 1β. The sign of each jump amplitude θ_i was chosen to drive, if possible, the protein into a favorable region of the Ramachadran plot. This was not possible when the average protein conformation was not a favorable one. In this case, the sign was chosen so as to get the calculated interproton NOEs in better agreement with the NOE experimental data. It is important to note, however, that the sign of θ_i does not influence the value of the calculated heteronuclear relaxation parameters.

2.3. Back-Calculation of NOESY Spectra of Flexible Protein Backbone Segments. Let M be the number of residues in the flexible backbone segment. In the case of crankshaft motions, the number of conformations of this segment is 2^M. Thus the flexible segments of calbindin and interleukin 1β have 16 and 32 conformations, respectively, and the respective rate constant matrix **T** is a 16 × 16 matrix for calbindin and a 32 × 32 matrix for interleukin 1β. By assuming similar conformer energies and satisfying the principle of detailed balance, the rate constant matrix **T** becomes symmetric. Each row and each column of the matrix contains M positive, off-diagonal elements. These elements are equal with the previously determined frequencies: $T_{JK} = \nu_i$, where the transition from the Kth to the Jth conformation refers to a conformer change at the ith residue. The diagonal elements are $T_{JJ} = -\sum_{i=1}^{2^M} \nu_i$. The above construction of the **T** matrix assumes that the conformer changes are independent from each other and there are no multiple changes simultaneously. The assumption of the independence

Protein Conformation and Dynamics

J. Phys. Chem. A, Vol. 103, No. 24, 1999 **4667**
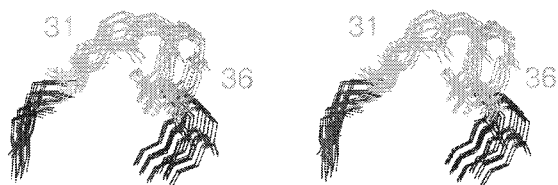
Figure 1. Stereoview of the superposition of the 32 conformers generated for interleukin 1β with the crankshaft motion model. For clarity, only the backbone atoms of the 29−38 region are shown. The 31−36 segment is highlighted in light gray.
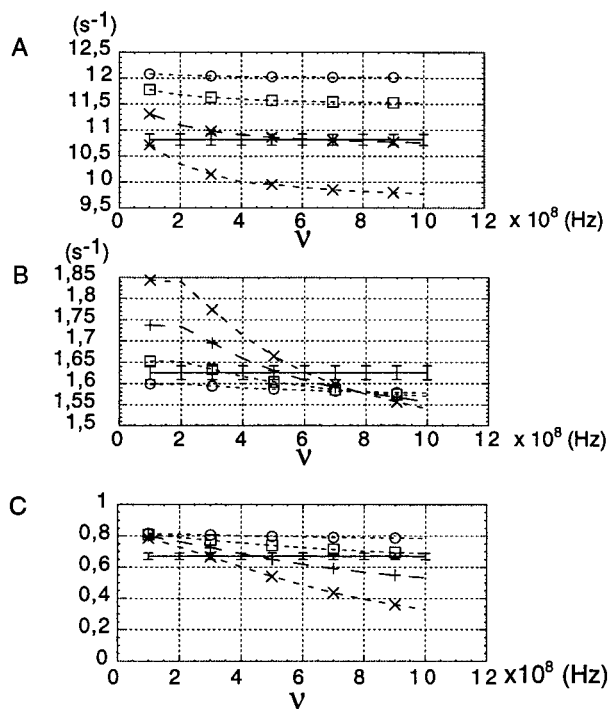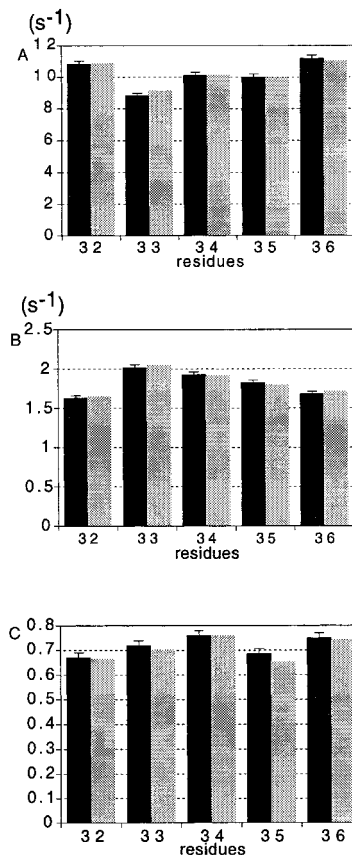

Figure 2. Simulation of the relaxation R_1, R_2, and NOE parameters using a two-state jump model as a function of the frequency ν for interleukin 1β: the correlation time used for calculations is 8.3 ns. The curves are drawn for different values of the amplitude θ. $\theta = 10°$ (○), $\theta = 20°$ (□), $\theta = 30°$ (+), $\theta = 40°$ (×).The values derived from experiments R_1 exp/S_{fast}^2, R_2 exp/S_{fast}^2, and NOE of Gln 32[18] are also depicted as horizontal solid lines.

Figure 3. ^{15}N relaxation parameters of the 32−36 region of interleukin 1β simulated using the jump model (gray boxes) versus the experimentally derived data, R_2 exp/S_{fast}^2, R_1 exp/S_{fast}^2, and NOE (black boxes). Crankshaft motions of Gln32, Gly33, Glu34, Asp35, and Met36 are of amplitude −28, −56, 47, 40, and −28° and of frequency 5×10^8, 1.7×10^8, 1.3×10^8, 2.5×10^8, 3×10^8 Hz, respectively. Key: (A) R_2; (B) R_1; (C) {^{1}H}−^{15}N NOE. Experimental ^{15}N relaxation data are taken from ref 18. Experimental schemes of acquisition are those described Kay et al. in ref 27.

is supported by all MD simulations reported to our knowledge for flexible parts of proteins.[8,10] As a consequence of these assumptions, the resulting $R_{1,jump}$, $R_{2,jump}$, and NOE$_{jump}$ for each residue are the same as the ones previously calculated using two conformations.

For simulating the NOESY spectra first the ^{1}H−^{1}H $\mathbf{R}_H$ relaxation matrix was constructed by using the eigensystem of the $2^M \times 2^M$ rate constant matrix $\mathbf{T}$ and eqs 2 and 5. The matrix exponential $L = \exp(-\mathbf{R}_H\tau_m)$ was constructed, by using the mathematical program libraries, Blas and Lapack, to diagonalize the relaxation matrix, $\mathbf{R}_H$. All spin diffusion processes are taken into account with this procedure. The accuracy of the calculations was checked by simulating a NOESY spectrum with mixing time $\tau_m = 0$ ms. The accuracy of NOE-based distance determination was found to be 0.02 Å. For graphical visualization, the output was in the Felix 95 format and plotted from there.

3. Results

The minimized average structures, derived from NOESY spectra, represent the global folding of interleukin 1β and calbindin.[20] The global folding is not affected by the crankshaft

type motions of the flexible segments of these proteins. The superposition of the 32 backbone conformers generated by the crankshaft motions of the region 31−37 for interleukin 1β is shown in Figure 1. Eventual bumps between the backbone atoms caused by the jumps were checked by using the Bump routine of InsightII (MSI, San Diego), and none was found. The crankshaft motions affect only the local backbone structure of the 31−37 segment of interleukin 1β and its close surroundings. Figure 1 shows that the peptidic plane of each residue in the 32−36 segment exists in two different conformations. The conformers are equally populated because each conformer is assumed to have similar energy.

Parts a−c of Figure 2 show for residue Gln32 the $R_{1,jump}(\nu)$, $R_{2,jump}(\nu)$, and NOE$_{jump}(\nu)$ curves, respectively, each calculated at four different jump amplitudes, θ, where ν, the frequency of the jump, is the independent variable. These curves were calculated by using eqs 1, 5, and 6. In Figure 2, the experimental values of R_1/S_{fast}^2, R_2/S_{fast}^2, and NOE relaxation parameters for the Gln32 residue of interleukin 1β are also shown (solid lines). The three relaxation parameters determine nicely and unambiguously both ν and θ, 5×10^8 Hz and 28°, respectively. A similar fitting procedure resulted in the following jump amplitudes and frequencies for each residue of the 32−36 segment: −28, −56, 47, 40, −28° and 5×10^8, 1.7×10^8, 1.1×10^8, 2.5×10^8, 3×10^8 Hz. Parts a−c of Figure 3 show the excellent agreement between the experimental relaxation parameters and the theoretical values calculated by using the above jump amplitudes

A

B
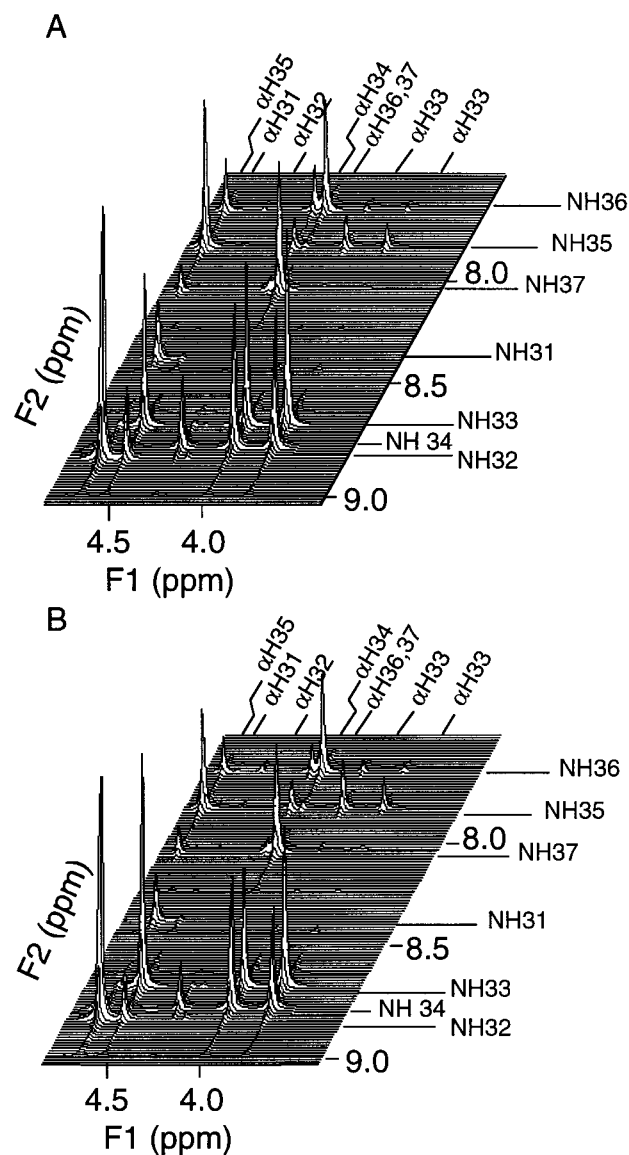
Figure 4. Simulated NOESY spectra of the 31−37 region of interleukin 1β showing the NH/αH dipolar correlations: (A) for the rigid model; (B) for the jump model. The calculations were performed with the relaxation matrix calculated for the whole protein, using a mixing time $\tau_m = 100$ ms. For clarity, only the resonances of interest are shown.

and frequencies. For each residue the deviation between the calculated and experimental values is below the maximal experimental error reported for similar measurements (as no error estimates are reported for interleukin 1β, we assumed a relative error of 2%, 2%, and 0.02 for R_1, R_2, and $\{^1H\}-^{15}N$ NOE, respectively). The good agreement between the calculated and experimental data strongly supports our interpretation for the relaxation parameters. The obtained jump amplitudes and frequencies define 32 configurations and their interconversion rates.

After determining the conformers and dynamics of the flexible segment of interleukin 1β, one can simulate the respective NOESY spectra as explained in section 2. The NH/αH portion of the NOESY spectrum simulated at mixing time 100 ms is shown in Figure 4b. For comparison, Figure 4a shows the simulated spectrum for the rigid, average conformation of interleukin 1β. It is clear from the comparison of the spectra in Figure 4 that there are no major differences in the heights of

TABLE 1: Comparison of the NOEs and Derived Distances Simulated for the 31−37 Segment of Interleukin 1β, Using the Flexible and Rigid Models[a]

	Leu 31	Gln 32	Gly 33	Gln 34	Asp 35	Met 36
NH_i/NH_{i+1}						
rigid model distance[b]	4.09	4.17	3.74	3.14	3.18	3.29
flexible model distance[b]	4.21	4.29	3.66	3.52	3.46	3.05
exp NOE[c]	w[e]	m	ND	sm	s	sm
$NOE_{flexible}/NOE_{rigid}$[d]	0.83	0.85	1.13	0.50	0.61	1.57
NH_i/NH_{i+2}						
rigid model distance				4.36	4.73	4.58
flexible model distance[b]				4.71	4.84	4.39
exp NOE[c]				ND	ND	ND
$NOE_{flexible}/NOE_{rigid}$[d]				0.63	0.87	1.30
NH_i/NH_{i+3}						
rigid model distance			4.66			
flexible model distance[b]			5.31			
exp NOE[c]			ND			
$NOE_{flexible}/NOE_{rigid}$[d]			0.34			
NH_i/NH_{i+4}						
rigid model distance		5.06				
flexible model distance[b]		5.75				
exp NOE[c]		ND				
$NOE_{flexible}/NOE_{rigid}$[d]		0.55				
$\alpha H_i/NH_{i+1}$						
rigid model distance	2.46	2.62	2.83−2.72	3.80	3.65	3.86
flexible model distance[b]	2.54	2.91	2.78−2.77	3.91	3.54	3.83
exp NOE[c]	M	s	sm	sm	m	ND
$NOE_{flexible}/NOE_{rigid}$[d]	0.85	0.54	1.12−1.13	0.85	1.20	1.05
$\alpha H_i/NH_{i+2}$						
rigid model distance			3.44−3.68	3.82	3.91	4.10
flexible model distance[b]			3.81−4.01	3.65	3.98	4.10
exp NOE[c]			mw	w	ND	ND
$NOE_{flexible}/NOE_{rigid}$[d]			0.60−0.55	1.32	0.90	1.00
$\alpha H_i/NH_{i+3}$						
rigid model distance			4.62−4.44	4.47	4.05	
flexible model distance[b]			5.05−5.19	4.67	4.02	
exp NOE[c]			ND	ND	ND	
$NOE_{flexible}/NOE_{rigid}$[d]			0.50−0.46	0.77	1.05	
$\alpha H_i/NH_{i+4}$						
rigid model distance		4.79				
flexible model distance[b]		5.76				
exp NOE[c]		ND				
$NOE_{flexible}/NOE_{rigid}$[d]		0.33				

[a] The correlation time used for calculation is 8.3 ns,[18] and the mixing time of the NOESY experiment, 100 ms.[21] [b] Distances calculated using the rigid and flexible models, respectively. [c] Experimental NOEs, taken from ref 21. They were collected on 2D homonuclear $^1H-^1H$ NOESY spectra and 3D heteronuclear ^{15}N NOESY HMQC spectra recorded on a 2.5 mM sample of ^{15}N-labeled interleukin 1β. [d] Ratios of the simulated NOEs using the flexible and the rigid models. [e] Key: s, strong; sm, strong-medium; m, medium; mw, medium-weak; w, weak; ND, non detected.

the most intense peaks. These are the peaks used to derive constraints for the determination of the average protein structure.
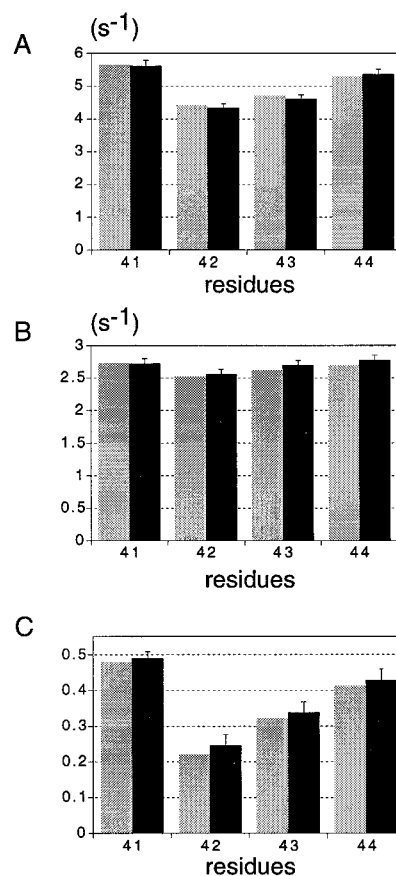
Table 1 lists the calculated NOEs for backbone atoms with interatomic distances $r < 5$ Å. The simulated NOEs, obtained from the flexible model, are in qualitative agreement with the experimental ones.[21] The NOE_{jump}/NOE_{rigid} ratio ranges from 0.33 to 1.57. Not surprisingly, the major deviations from unity are found for residues undergoing the largest amplitude motions, and they are also the residues that are the most mobile ones according to the model-free analysis of their relaxation data. The distances in Table 1 were calculated from the NOEs by using an external theoretical peak reference,[29] which ensures that the distance differences in Table 1 are the theoretically minimal differences.[11] Taking a simulated peak as a reference

Protein Conformation and Dynamics

J. Phys. Chem. A, Vol. 103, No. 24, 1999 **4669**
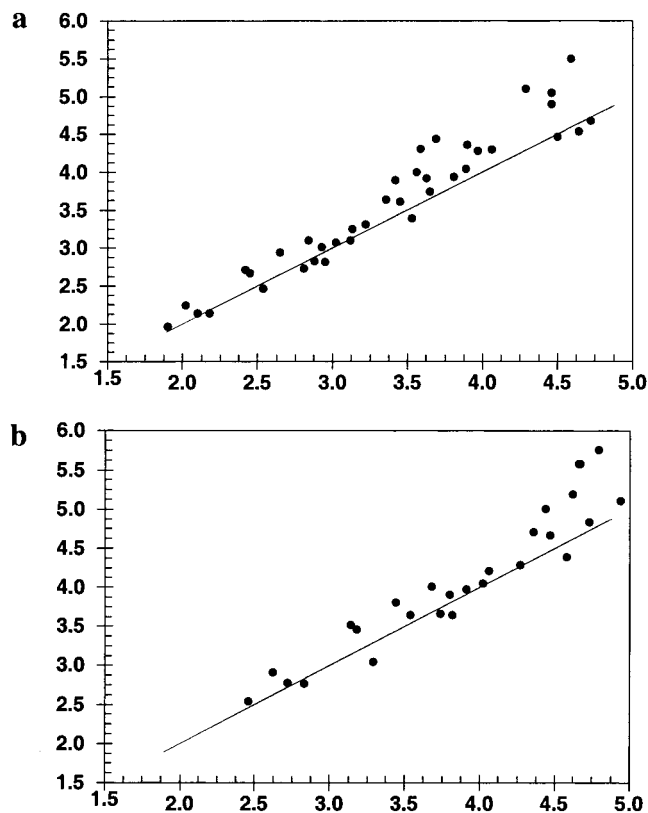
Figure 5. Plot of the NOE derived distances with the flexible model versus the rigid model for interleukin 1β using (a) an external theoritical peak reference and (b) the calculated NOE effect between the geminal protons of Cys 8 as reference. For all calculations, the mixing time of the NOESY experiment was set to 100 ms.

Figure 6. ^{15}N relaxation parameters of the $41-44$ region of calbindin D_{9k} simulated using the jump model (gray boxes) versus the experimentally derived data[19] (black boxes), R_2 exp/S_{fast}^2, R_1 exp/S_{fast}^2, and NOE. Crankshaft motions of Lys 41, Gly 42, Gly43, and Ser 44 are of amplitude 44, 72, 69, and 48° and of frequency 3.6×10^8, 3.6×10^8, 3.2×10^8, and 3.3×10^8 Hz. Key: (A) R_2; (B) R_1; (C) {^{1}H}$-^{15}$N NOE. Experimental ^{15}N relaxation data are taken from ref 19. Experimental schemes of acquisition are those described by Skelton et al. in ref 28.

peak would probably increase the differences because of the spin diffusion. From the relationship $|\Delta r/r| = {}^1/_6|(\Delta NOE/NOE)$ it follows that for the same variation of NOEs, the major distortions in distance determination appear for those protons that are far from each other, i.e., for protons with small respective NOEs. Indeed, in Table 1, the maximum distortion in distance determination, 0.97 Å, is found for the distance between the αH proton of Gln 32 and the NH proton of Met 36, resulting from a 33% decrease of the respective NOE. The mean distance bias for strong NOEs is 0.08 Å, for medium NOEs 0.22 Å, and for weak NOEs 0.31 Å, while the overall mean distance distortion is 0.29 Å.

The model dependent differences are mainly in the intensities of the minor peaks (see Table 1). All of these peaks belong to nonsequential residues: HN 36/HN 32; HN 34/HN 36; HN 35/ HN 33; HN 36/HN 33; HN 35/HN 32; HN36/H$\alpha_1$33, HN 36/ Hα_2 33; HN 35/Hα_1 33; HN 35/Hα_2 33; HN 36/Hα 32, HN 36/Hα 34, HN 34/Hα 31, HN 37/Hα 35. In this list of non sequential NOEs, only the NOEs HN 35/Hα_1 33, HN 35/Hα_2 33, and HN 36/Hα 34 are reported to be present in the experimental spectra, with a medium$-$weak and weak intensities, respectively. The respective interproton distances derived from the simulation using the rigid model ($3.44-3.68$ and 3.82) seem to be in better agreement with the distances obtained from experimental NOEs than the distances derived from NOEs of the flexible model ($3.81-4.01$ and 3.65). However, for all the experimentally undetected nonsequential NOEs, the NOE$_{jump}$/ NOE$_{rigid}$ ratio is less than 1 (except for NH 36/NH 38 and αH 35/NH 38). Although these peaks are still present in the simulated spectra of the flexible model, it is likely that the experimental noise prevents their detection.

Parts a and b of Figure 5 compare the distances derived from the spectra simulated using the flexible and rigid models with an external peak and an internal peak as reference, respectively. To limit the spin diffusion effect as much as we can, we chose the peak between the geminal β protons of Cys8 as an internal reference. Only distances below 6 Å were taken into account. Calibration with this internal reference peak resulted in an overall underestimation of distances. But, independently from the type of the reference, the effects of the models remain similar. The introduced flexibility decreases generally the NOEs, i.e., increases the derived distances, and this phenomenon is more pronounced at larger distances. Our simulation also shows that the difference between the distance obtained from the flexible and rigid models is more pronounced when distances are derived from an internal reference peak; i.e., the rigid model underestimates the distances in the range of $3.5-5$ Å if one takes an internal peak as reference (see Figure 5b), while in the case of an external reference, the underestimation is obvious in the range of $4-5$ Å (see Figure 5a).

We also investigated the effect of calculating the spectral density in different ways on the simulated spectra. The spectral densities of protons in the $31-36$ segment of interleukin 1β were calculated by means of the (i) exact jump dynamics, (ii) static $\langle r^{-6}\rangle$ averaging over the conformers, and (iii) more "dynamic" $\langle r^{-3}\rangle^2$ averaging over the conformers. Each of these simulations was performed at zero mixing time. Thus there is

TABLE 2: Comparison of the NOEs and Derived Distances Simulated for the 39−44 Segment of Calbindin D$_{9k}$, Using the Flexible and Rigid Models[a]

	Ser 38	Leu 39	Leu 40	Lys 41	Gly 42	Gly 43	Ser 44
NH$_i$/NH$_{i+1}$							
rigid model distance[b]	3.02	3.62	3.30	2.97	3.71	2.40	4.35
flexible model distance[b]	3.03	3.61	3.58	3.67	3.90	2.46	4.51
exp NOE[c]	4.6	3.2	ND[e]	3.8	5.5	3.1	ND
NOE$_{flexible}$/NOE$_{rigid}$[d]	1.00	1.01	0.61	0.28	0.75	0.87	0.82
NH$_i$/NH$_{i+2}$							
rigid model distance	4.24	4.92	4.49		4.35		
flexible model distance[b]	4.23	5.41	5.38		4.41		
exp NOE[c]	3.2	ND	ND		ND		
NOE$_{flexible}$/NOE$_{rigid}$[d]	1.01	0.56	0.34		0.92		
αH$_i$/NH$_{i+1}$							
rigid model distance	3.90	4.06	3.94	3.80	3.09−2.88	3.26−3.16	2.78
flexible model distance[b]	3.90	4.05	4.12	3.74	3.16−2.97	3.33−3.30	2.79
exp NOE[c]	3.2	ND	ND	3.8	4.6	4.6	5.5
NOE$_{flexible}$/NOE$_{rigid}$[d]	1.00	0.567	0.77	1.11	0.87−1.04	0.94−0.74	1.00
αH$_i$/NH$_{i+2}$							
rigid model distance	4.82	4.40		4.53	3.69−3.32		
flexible model distance[b]	4.83	5.05		5.38	3.63−3.34		
exp NOE[c]	4.2	5.5		ND	0		
NOE$_{flexible}$/NOE$_{rigid}$[d]	1.00	0.44		0.36	1.10−0.97		
αH$_i$/NH$_{i+3}$ rigid model distance	4.53	3.81		4.26			
flexible model distance[b]	4.90	4.66		5.34			
exp NOE[c]	5.5	ND		ND			
NOE$_{flexible}$/NOE$_{rigid}$[d]	0.62	0.297		0.258			

[a] The correlation time used for calculation is 4.25 ns,[19] and the mixing time of the NOESY experiment, 200 ms. [b] Distances calculated using the rigid and flexible models, respectively. [c] Experimental NOEs (Dr. Walter Chazin, personal communication). They were collected on 2D homonuclear ^{1}H−^{1}H NOESY spectra recorded on a 5 mM sample of calbindin D$_{9k}$. [d] Ratios of the NOEs simulated using the flexible and the rigid models. [e] ND: nondetected.

no spin diffusion involved in the following results. Because the $\langle r^{-6} \rangle$ and $\langle r^{-3} \rangle^2$ averaging take into account conformational flexibility, it is expected that the corresponding average distances are closer to the distances obtained from the flexible than the rigid model. For interleukin 1β, the root mean square (rms) deviation of the interproton distances obtained from the flexible model with the distances obtained with the $\langle r^{-3} \rangle^2$ averaging is 0.23 Å while the rms deviation with the distances obtained with the $\langle r^{-6} \rangle$ averaging is 0.27 Å. The maximal distance deviation for $\langle r^{-3} \rangle^2$ averaging was found for the HN 35/HN 37 distance calculated to be 5.38 Å with the flexible model versus 4.94 Å with the $\langle r^{-3} \rangle^2$ averaging, i.e., 0.44 Å. This is to be compared to the maximal deviation of 0.94 Å found between rigid and flexible models. Not surprisingly, introducing dynamical averaging reduces the maximal distance distortion caused by mobility by a factor 2.

The above-described calculations were repeated to investigate the 41−44 segment of the calbindin protein. ^{15}N relaxation data suggested the occurrence of crankshaft motions in this segment. A good fit of the calculated and observed ^{15}N relaxation parameters was obtained by using the model of crankshaft motions with amplitudes θ of 44, 72, 69, and 48° and jump frequencies of 3.6×10^8, 3.6×10^8, 3.2×10^8, and 3.3×10^8 Hz. Figure 6 shows good agreement between the calculated relaxation parameters and the experimental ones. In Table 2 experimental (Dr. Walter Chazin, personal communication) and calculated ^{1}H−^{1}H NOEs are listed. The calculated NOEs were obtained from both the rigid and the flexible models. In every case, the flexible model was a better predictor of the experimental NOE than the rigid model. The most striking model dependent differences for nonsequential NOEs were found for the αH 39/HN 43 and αH 41/HN 44 contacts, which were not experimentally detected, and whose NOE$_{jump}$/NOE$_{rigid}$ ratios are 0.3 and 0.26, respectively. The respective interproton distances calculated from the rigid model are 3.81 and 4.26 Å, while from

the flexible model they are 4.66 and 5.34 Å. The larger interproton distances, predicted by the flexible model, explain why the NOEs were experimentally not detected. As we noted above, the larger interproton distances, i.e., the weaker NOEs, are affected mostly by the model we use. In our example for calbindin, the rigid model incorrectly predicts most of the medium−weak, nonsequential NOEs, while in the case of the flexible model these peaks are probably buried under the noise level.

4. Discussion and Conclusion

In this paper the effects of crankshaft type motions on the interproton cross-relaxation rates are investigated. We focus on this type of anticorrelated motions, because, according to MD simulations, they are the main relaxation active processes in flexible loops of proteins. It is important to note that for constrained cyclic peptides the assumption of crankshaft motions is not valid, since MD simulations on anthanamide showed that distortions of the backbone exhibit a variable degree of anticorrelation.[22] We assume that the conformers, of the flexible loop are equally populated. To determine the population of the conformers, one would need to measure at least another relaxation parameter. Unfortunately, the commonly measured relaxation parameters, such as the ^{1}H$_z$^{N}N$_z$ and ^{1}H$_z$^{N}N$_x$ rates, are not reliable enough for our purpose because of the presence of proton relaxation leakage. However, we note that the recent advances in the measurement of new relaxation parameters of ^{15}N and ^{13}C atoms could alleviate this problem.[23]

The conformers and dynamics of flexible protein segments were determined according to the following protocol. Short flexible segments of interleukin 1β and calbindin were previously identified by analyzing the respective experimental heteronuclear relaxation data.[17,18] The overall correlation time and the order parameter of the librational motions of the N−H vectors were those previously extracted by means of the

Protein Conformation and Dynamics

J. Phys. Chem. A, Vol. 103, No. 24, 1999 **4671**

extended model-free approach.[17,18] Then, the parameters of the crankshaft motions (amplitudes and frequencies) were determined separately for each residue by fitting the simulated ^{15}N heteronuclear relaxation data to the experimental ones. We investigated the effects of the crankshaft motions on the homonuclear proton NOEs. The presence of crankshaft type motions can affect $^1H-^1H$ NOEs so that the derived distances may increase by up to 1 Å for the weakest NOEs, while the intensity of strong cross-peaks was only slightly affected. Our analysis shows that strong NOEs back-calculated from the rigid average structure are very likely present in the experimental NOESY spectra. On the other hand, NOEs corresponding to distances around 4 Å can be absent from the experimental NOESY spectra due to the intramolecular motions. We think that the assumption of equally populated conformers does not affect this general conclusion. Assuming the second population less populated than the original one would obviously lead to jumps of larger amplitude, so that the minor weight of the NOEs stemming from this second population would be counterbalanced by their more drastic difference. For sake of clarity and simplicity, our present investigation has focused on NOEs of backbone protons. The effects of backbone crankshaft motions would be more pronounced for side chain atoms, due to the superposition of intra-side-chain motions. It is important to note that a recent study by Bremi et al.[24] showed that NMR relaxation data for side chains of phenylalanines in antanamide can be described by Gaussian axial fluctuations superimposed by lattice jump motions, referred to as the GAF and Jump model. This approach is very similar to ours, from the conceptual point of view, in separating the relaxation active processes; however, Bremi et al. are particularly interested in characterizing precisely the fast motions. The work presented by us is closer to the so-called "collective NMR relaxation model" of Bruschweiler and Case,[25] which is based on normal mode dynamics incorporating the heteronuclear relaxation data as restraints. In contrast to our study, this approach was restricted to the investigation of fast fluctuations of $\tau_{internal} < 50$ ps. LeMaster[11] recently investigated motions of the N–H vectors on interproton distance determination. His work was based on simulations where the N–H and/or C–H vectors were allowed to freely diffuse into a cone or exchange between two conformations provided the resulting simulated order parameter S^2 reproduced the experimentally derived one. This investigation was also limited to fast motions, while our approach is valid for a broad time scale of motions.

Finally, we investigated the effect of calculating the spectral density in different ways on the simulated spectra. The exact method using the interconversion rates between conformers was compared with the more static methods using $\langle r^{-6}\rangle$ and $\langle r^{-3}\rangle^2$ averaging among conformers. It was shown that the static averaging methods provide better results than the rigid model, but they still underestimate the effect of flexibility in NOE simulation. It was found that $\langle r^{-3}\rangle^2$ averaging provides NOEs in better agreement with the exact method than $\langle r^{-6}\rangle$ averaging. This is the case because $\langle r^{-6}\rangle$ averaging should be used only when the equilibration between conformers is slower than the overall correlation time of the molecule. $\langle r^{-3}\rangle^2$ averaging on the other hand is applicable when the equilibration of the conformers is faster than the overall correlation time. In the case of interleukin 1β and calbindin, the overall tumbling is slower than the time scale of the crankshaft motions which explains the success of the $\langle r^{-3}\rangle^2$ averaging.

The precision of conversion of NOEs into distance restraints has been widely debated.[26] Currently, the general tendency is to construct the largest set of experimentally derived constraints with loose upper and lower bounds. The present study shows that the distance constraints can be tightened for those segments of proteins where only limited conformational flexibility, i.e., librational vibrations, is revealed by heteronuclear NMR relaxation measurements.

References and Notes

(1) (a) Landry, S. J.; Taher, A: Georgopoulos. C.; van der Vies, S. M. *Proc. Natl. Acad. Sci. U.S.A.* **1996**, *93*, 11622−11627. (b) Ye, X.; Gorin, A.; Ellington, A. D.; Patel, D. J. *Nat. Struct. Biol.* **1996**, *96*, 3, 1026−1033.

(2) Koning, T. G. M.; Boelens, R.; Kaptein, R. *J. Magn. Reson.* **1990**, *90*, 111−123.

(3) Kemming, J.; Scheek, R. M. *J. Biomol. NMR* **1995**, *5*, 33−40.

(4) (a) Landis, C.; Allured, V. S. *J. Am. Chem. Soc.* **1991**, *113*, 9493−9499. (b) Brüschweiler, R.; Blackledge, M.; Ernst, R. R. *J. Biomol. NMR* **1991**, *1*, 3−11. (c) Blackledge, M. J.; Bruschweiler, R.; Griesinger, C.; Xu, P.; Ernst, R. R. *J. Am. Chem. Soc.* **1993**, *32*, 10960−10974. (d) Cicero, D. O.; Barbato, G.; Bazzo, R. *J. Am. Chem. Soc.* **1995**, *117*, 1027−1033. (e) Ulyanov, N. B.; Schmitz, U.; Kumar, A.; James, T. L. *Biophys. J.* **1995**, *68*, 13−24.

(5) Lipari, G.; Szabo, A. J. A. J. *Am. Chem. Soc.* **1982**, *104*, 4546−4559.

(6) (a) Koenig, T. M. G.; Boelens, R.; van der Marel, G. A.; van Boom, J. H.; Kaptein, R. *Biochemistry* **1991**, *30*, 3787−3797. (b) Lommerse, J. P. M.; Kroon-Batenburg, L. M. J.; Kroon, J.; Kamerling, J. P.; Vliegenthart, J. F. G *J. Biomol. NMR* **1995**, *5*, 79−94.

(7) (a) Torda, A. E.; Scheek, R. M.; van Gunsteren, W. F. *Chem. Phys. Lett.* **1989**, *157*, 289−294. (b) Torda, A. E.; Scheek, R. M.; van Gunsteren, W. F. *J. Mol. Biol.* **1990**, 214, 223−235. (c) Pearlman, D. A.; Kollman, P. A. *J. Mol. Biol.* **1991**, *220*, 457−479. (d) Kemming, J.; Scheek, R. M. *J. Biomol. NMR* **1995**, *5*, 33−40. (e) Cuniasse, P.; Raynal, I.; Yiotakis, A.; Dive, V. *J. Am. Chem. Soc.* **1997**, *119*, 5239−5248. (f) Schneider, T. R.; Brünger, A. T.; Nilges, M. *J. Mol. Biol.* **1998**, *285*, 727−740.

(8) (a) Chandrasekhar, I.; Clore, G. M.; Szabo, A.; Gronenborn, A. M.; Brooks, B. R. *J. Mol. Biol.* **1992**, *226*, 239−250. (b) Eriksson, M. A. L.; Berglund, H.; Härd, T.; Nilsson, L. *Proteins: Struct. Funct. Genet.* **1993**, *17*, 375−390. (c) Fushman, D.; Ohlenschläger, O.; Rüterjans, H. *J. Biomol. Struct. Dyn.* **1994**, *11*, 1377−1402. (d) Lienin, S. F., Bremi, T.; Brutscher, B.; Brüschweiler, R.; Ersnt, R. R. *J. Am. Chem. Soc.* **1998**, *120*, 9870−9879. (e) Smith, L. J.; Mark, A. E.; Dobson, C. M.; Van Gunsteren, W. F. *Biochemistry* **1995**, *34*, 10918−10931. (f) Yamasaki, K.; Saito, M.; Oobatake, M.; Kanaya, S. *Biochemistry* **1995**, *34*, 6587−6601.

(9) Smith, P. E.; van Scheik, R. C.; Szyperski, T.; Wutherich, K.; van Gunsteren, W. F. *J. Mol. Biol.* **1995**, *246*, 356−365.

(10) (a) Wittebort, R. J.; Szabo, A. *J. Chem. Phys.* **1977**, *69*, 1722−1736. (b) Sugàr, I. P. *J. Phys. Chem.* **1992**, *96*, 10719−10724.

(11) LeMaster, D. M. *J. Biomol. NMR* **1997**, *9*, 79−93.

(12) Clore, G. M.; Szabo, A.; Bax, A.; Kay, L. E.; Driscoll, P.; Gronenborn, A. M. *J. Am. Chem. Soc.* **1990**, *112*, 4989−4991.

(13) (a) MacCammon, J. A.; Gelin, B. R.; Karplus, M. *Nature* **1977**, *267*, 585−590. (b) Levitt, M. *J. Mol. Biol.* **1983**, *168*, 621−657. (c) Wasserman, Z. R.; Salemme, F. R. *Biopolymers* **1990**, *29*, 1613−1631. (d) Fadel, A. R.; Jin, D. Q.; Montelione, G. T.; Levy, R. M. *J. Biomol. NMR* **1995**, *6*, 221−226.

(14) Abragam, A. *The Principles of Nuclear Magnetic Resonance*; Clarendon Press: Oxford, England, 1961; pp 289−316.

(15) Hiyami, Y.; Niu, C. H.; Silverton, J. V.; Bavoso, A.; Torchia, D. A. *J. Am. Chem. Soc.* **1988**, *110*, 2378−2383.

(16) Tropp, J. *J. Chem. Phys.* **1980**, *72*, 6035−6043.

(17) Rose, M. E. *The Elementary theory of Angular Momentum*; Wiley: New York, 1957; Chapter 4.

(18) Clore, G. M.; Driscoll, P. C.; Wingfield, P. T.; Gronenborn, A. M. *Biochemistry* **1990**, *29*, 7387−7401.

(19) Kordel, J.; Skelton, N. J.; Akke, M.; Palmer, A. G.; Chazin, W. J. *Biochemistry* **1992**, *31*, 4856−4866.

(20) (a) Clore, G. M.; Wingfield, P. T.; Gronenborn, A. M. *Biochemistry* **1991**, *30*, 2315. (b) Kördel, J.; Skelton, N. J.; Akke, M.; Chazin, W. J. *J. Mol. Biol.* **1993**, *231*, 711−734.

(21) Driscoll, P. C.; Gronenborn, A. M.; Wingfield, P. T.; Clore, G. M. *Biochemistry* **1990**, *29*, 4668−4682.

(22) Bremi, T.; Bruschweiler, R.; Ernst, R. R. *J. Am. Chem. Soc.* **1997**, *119*, 6672.

(23) (a) Dayie, K. T.; Wagner, G. *J. Magn. Reson*. **1995**, *109B*, 105–108. (b) Cordier, F.; Brutscher, B.; Marion, D. *J. Biomol. NMR* **1996**, *7*, 163–168. (c) Tjandra, N.; Szabo, A.; Bax, A. *J. Am. Chem. Soc*. **1996,** *118*, 6986–6991. (d) Zeng, L.; Fischer, M.; Zuiderweg, E. R. P. *J. Biomol. NMR* **1996**, *7*, 157–162. (e) Fischer, M. W. F.; Zeng, L.; Pang, Y.; Hu, W.; Majumdar, A.; Zuiderweg, E. R. P. *J. Am. Chem. Soc*. **1997**, *119*, 12629–12642.

(24) Bremi, T.; Bruschweiler, R.; Ernst, R. R. *J. Am. Chem. Soc*. **1997,** *119*, 4272–4284.

(25) Bruschweiler, R.; Case, D. A. *Phys. Rev. Letts*. **1994**, *72*, 940–943.

(26) (a) Thomas, P. D.; Basus, V. J.; James, T. L. *Proc. Natl. Acad. Sci. U.S.A*. **1991**, *88*, 1237–1241. (b) Clore, G. M.; Robien, M. A.; Gronenborn, A. M. *J. Mol. Biol*. **1993**, *231*, 82–102. (c) Zhao, D.; Jardetzky, O. *J. Mol. Biol*. **1994**, *239*, 601–607. (d) Hoogstraten, C. G.; Markley, J. L. *J. Mol. Biol*. **1996**, *258*, 334–348.

(27) Kay L. E.; Torchia, D. A.; Marion, D. *Biochemistry* **1989**, *28*, 8972–8979.

(28) Skelton, N. J.; Palmer, A. G.; Akke, M.; Kördel, J.; Chazin, W. J. *J. Magn. Reson., Ser. B* **1993**, *102*, 253–264.

(29) To derive a distance from a NOE, one has to calibrate it to a reference NOE corresponding to a known distance. By external threoretical peak reference, we mean the theoritical NOE by contrast to a NOE taken from the spectra (either simulated or experimental).